Spatial Variability of Particulate Matter and Sources

3. Mobile Laboratory Observations of Temporal and Spatial Variability within the Coastal Urban Aerosol

i. Introduction

Particulate matter (PM) has been shown to negatively impact human health over short and long term periods of exposure (96-98). Short term effects from elevated levels of particulate matter have also been observed, including increased hospital admissions for asthma, cardiovascular disease, and chronic obstruction pulmonary disease on days where PM less than 10 micrometers (PM_{10}) increased by 10 $\mu g/m^3$ (97). For example, at a series of hospitals in Utah, a recent study showed that a 10 $\mu g/m^3$ increase in $PM_{2.5}$ increased the risk of ischemic heart disease events (e.g. heart attacks) by 4.5% in patients (99). Long term studies have shown connections between particulate matter and lung cancer, cardiopulmonary mortality, and cardiovascular disease (97,98). Orru et al. found that the impact of particulate matter on human health had high spatial variability based on varying exposure levels to $PM_{2.5}$ in different neighborhoods throughout an urban environment (100). In addition to the mass concentration of PM present, negative health effects have also been linked to both particle size and chemical composition (97,98,101). Particle size plays a key role in determining where and to what extent inhaled particles deposit in the tracheobronchial and pulmonary systems (102-104). Where particles deposit in the body is also impacted by the degree to which particles grow when exposed to high relative humidity after inhalation, which is determined by particle size and chemical composition (102). In addition, single particle mixing state of particles plays a role in the negative health effects from particles. Synergistic effects have been shown when specific species are present together such as oxidative stress and NFκB activation (iron and soot), as well as cardiovascular and thermoregulatory effects (vanadium and nickel) (65,105). Thus, the health effects of PM are dependent on particle concentrations, size, and chemical composition.

As size, chemical composition, temporal variability, and spatial variability all contribute to the negative health effects of particulate matter, detailed measurements assessing these variables are necessary to understand and address this unique problem. However, understanding the urban aerosol has long been a challenge for aerosol researchers due to the complexity and the rapidly evolving nature of urban environments. For example, even determining the optimal metric for relating atmospheric measurements and human health has been challenging as basic parameters, such as particle number concentration and mass, do not always track each other (106). The merits of particle size distributions based on number concentration (107,108), surface area (109), and mass (110) have all been discussed as possibilities for linking particulate matter and health, but much is still unknown as to the causal link in ambient conditions. Increasing the understanding of urban aerosols is one portion of decreasing the uncertainty of the particle-health link and many studies have looked at both the long and short term trends in particle properties in an urban environment (111-116).

One of the more challenging aspects of decreasing uncertainty between exposure and health is determining the spatial variability of aerosols in an urban area. Three main

approaches have been utilized to measure aerosol spatial variability: multiple sampling sites operating simultaneously, models incorporating data from one or more sites, and mobile/portable laboratories. For instance, Mejia et al. compared measurements at 8 sites in Brisbane, Australia and found considerable variability in number concentrations and size distributions (depending on which whether the vehicle fleet was primarily cars or trucks) (117). Krudysz et al. monitored 13 sites around the Ports of Los Angeles and Long Beach and also found spatial variability in particle concentrations and size distributions, especially among ultrafine particles (111,117). When operating multiple sites continuously particle chemistry is often measured with only low resolution filter techniques. Models also have been used to expand the reach of studies with one or more sampling sites through meteorological or chemical mass balance models (118,119). Recently, many portable and/or mobile laboratories have been developed which can monitor and move quickly between sampling locations or sample while moving, which gives both high temporal and spatial resolution (120,121). Many of these laboratories have focused on fresh vehicle emissions (122-125) or spatial patterns of specific species (i.e. hexavalent chromium) (126). Herein, this paper will discuss measurements involving the development and deployment of the mobile aerosol time-of-flight mass spectrometry (ATOFMS) laboratory. These measurements of spatial and temporal variability with real-time particle size and chemistry mark the first single particle mass spectrometry measurements at multiple sites in a single day, providing particle concentrations, sizes, and chemistry that can be incorporated into future health studies.

ii. Experimental

a. Mobile ATOFMS Laboratory

A Pace American Class IV trailer (length 5.5 m; width 3.5 m; height 3 m; maximum gross trailer weight 4,500 kg) was modified to house an array of gas phase and aerosol instrumentation. The mobile ATOFMS laboratory was transported between sites by a Chevrolet Silverado 3500 pickup truck equipped with two Honda EB11000 gasoline generators (9.5 kVA) supported by a steel frame anchored to the truck bed. The generator exhaust passed through an exhaust manifold and 20 m of 6 cm diameter steel tubing to transport the emissions downwind of the sampling inlet. One generator was capable of powering the trailer at full load for 3-4 hours under normal operating conditions on a single tank of gas. This study focused on stationary sampling and at each site a 2.5 meter sampling line was attached to a sampling manifold on the mobile ATOFMS laboratory roof (5.5 meters above the ground). The manifold provided laminar sampling flow for 5-6 instruments in parallel with similar residence times.

b. 2009 San Diego Bay Measurements

The mobile ATOFMS laboratory sampled the urban aerosol at multiple locations around San Diego Bay on both February 12 and March 13, 2009. Sampling times and locations are provided in **Table 5** and **Figure 19**. On February 12th, sampling was conducted at three locations: Silver Strand State Beach (SS), Cesar Chavez Park (CC) in downtown San Diego, and Coronado Tidelands Park (Cor). These same three sites were sampled on March 13th, as well as Chula Vista Bayfront Park (CV) and Pepper Park (Pep) in National City. Throughout this paper SS1, CC1, and Cor1 refer to the

measurements at the three sites on February 12th and SS2, Cor2, CC2, CV2, and Pep2 reference the measurements made on March 13th.

Site	Abbreviation	Latitude (°N)	Longitude (°W)	Sampling Start	Sampling Stop
Silver Strand	SS1	32° 37' 58"	117° 08' 29'	2/12/2009 9:48	2/12/2009 12:18
Cesar Chavez Park	CC1	32° 41' 46"	117° 09' 01"	2/12/2009 14:21	2/12/2009 16:10
Coronado	Cor1	32° 41' 28"	117° 09' 58"	2/12/2009 17:26	2/12/2009 19:09
Silver Strand	SS2	32° 37' 58"	117° 08' 29"	3/13/2009 8:29	3/13/2009 10:20
Coronado	Cor2	32° 41' 28"	117° 09' 58"	3/13/2009 11:41	3/13/2009 13:03
Cesar Chavez Park	CC2	32° 41' 46"	117° 09' 01"	3/13/2009 13:57	3/13/2009 15:02
Chula Vista Park	CV2	32° 37' 11"	117° 06' 11"	3/13/2009 16:10	3/13/2009 17:03
Pepper Park	Pep2	32° 39' 02"	117° 06' 38"	3/13/2009 18:35	3/13/2009 20:02

Table 5: Sampling times and locations at sites around San Diego Bay are described.

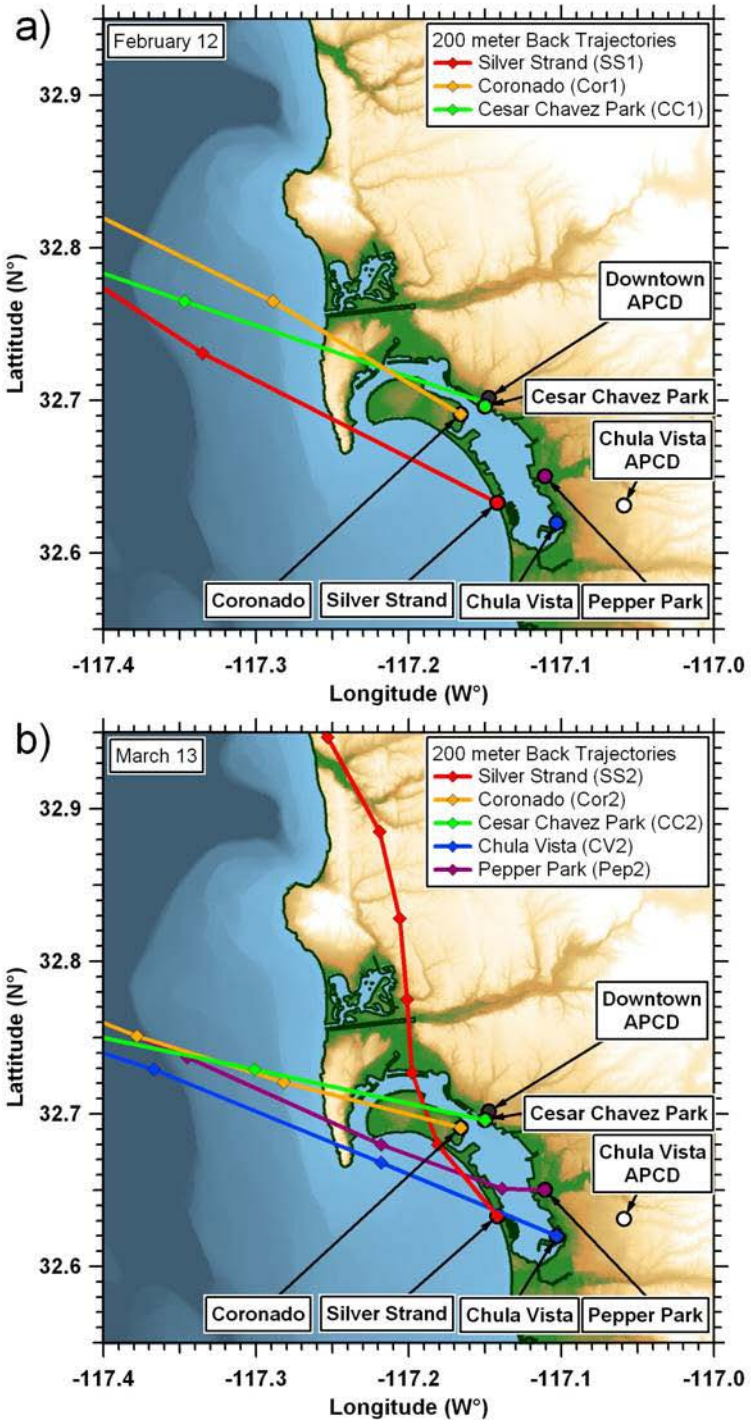

Figure 19: Map of the San Diego metropolitan area around San Diego Bay with trailer sampling sites and air pollution control district (APCD) sites, as well as 200 meter HYSPLIT air mass back trajectories for (a) February 12, 2009 and (b) March 13, 2009.

c. Instrumentation

Standard aerosol instrumentation in the mobile ATOFMS laboratory included $PM_{2.5}$ mass concentrations from a beta attenuation monitor (BAM) (MetOne Model

BAM-1020) and black carbon mass concentrations from a seven wavelength aethalometer (Model AE31, Magee Scientific). Aerosol size distributions were collected between 0.011 - 0.604 μm by a scanning mobility particle sizer (SMPS) (Model 3936L, TSI Inc.) and 0.523 -10 μm by an aerodynamic particle sizer (APS) (Model 3321, TSI Inc.). Measurements of meteorology, gas phase concentrations, and mass concentrations ($PM_{2.5}$) were also incorporated from San Diego Air Pollution Control District (SD-APCD) sites in downtown San Diego (DT-APCD), Chula Vista (CV-APCD), and at the San Diego International Airport (SDAP).

d. Aerosol Time-of-Flight Mass Spectrometry

An ATOFMS was operated inside the mobile laboratory measuring the size and chemical composition of individual particles between 0.2-3.0 μm in real-time at each site. The design and details of the ATOFMS have been described in detail previously (127). Briefly, particles are introduced into the ATOFMS through a converging nozzle into a differentially pumped vacuum chamber where the particles are accelerated to a size dependent velocity. The particles pass through two continuous wave lasers (diode pumped Nd:YAG lasers operating at 532 nm) located 6 cm apart. Particle speed is used to determine vacuum aerodynamic diameter by calibration with polystyrene latex spheres of known size. The sized particles are desorbed and ionized in the mass spectrometer source region by a 266 nm Q-switched Nd:YAG laser (1.2-1.4 mJ). Positive and negative ions from the same single particle are detected using a dual-reflectron time-of-flight mass spectrometer.

e. Single Particle Data Analysis

Single particle size and mass spectral information were analyzed with YAADA 1.2 (www.yaada.org), a data analysis toolkit for MATLAB 6.5.1 (The MathWorks, Inc.). Particles were analyzed via two approaches: 1) searching mass spectral, aerodynamic size, and temporal features and 2) clustering mass spectra using an Adaptive Resonance Theory based neural network algorithm (ART-2a) at a vigilance factor of 0.8 (35). ART-2a combines particles into clusters based on the intensity of ion peaks in individual mass spectra. General particle types are defined by the characteristic chemical species or possible source to simplify the naming scheme; these labels do not reflect all of the species present within a specific particle type, but reflect the most intense ion peaks. Peak identifications within this paper correspond to the most probable ions for a given m/z ratio.

f. Scaling Single Particle Measurements to Mass Concentrations

Number and mass concentrations were calculated for different particle types using APS size-resolved number concentrations, which has been shown previously to yield quantitative mass concentrations (128). Briefly, ATOFMS counts are divided into APS size bins (0.523 – 2.5 μm) and scaling factors were calculated for each site to account for ATOFMS transmission biases. Bins with less than 10 particles at a site were excluded due to low statistics, which might lead to slight undercounting of PM_1 and $PM_{2.5}$. After scaling to number concentration, mass was calculated using a representative density for particles in an urban atmosphere that have taken up water and secondary species, 1.5 g/cm^3 (129). Scaled ATOFMS mass concentrations have been shown previously to

correlate well with standard mass measurements and comparisons to the BAM $PM_{2.5}$ mass concentrations are included below (128). Previous ATOFMS measurements in San Diego used scaled mass concentrations to determine the impact of transported particles from the Los Angeles port region, demonstrating the utility of the method locally (74).

iii. Results and Discussion

a. Temporal Patterns of Meteorological and Gas Phase Concentrations

To characterize the ambient conditions on February 12th and March 13th the meteorological and gas phase concentrations of each day are compared (**Figure 20**). The meteorological conditions recorded at the DT-APCD on both February 12th and March 13th had normal diurnal trends in temperature (red line – peaking late morning) and relative humidity (RH) (light blue line – minima midday). RH was monitored at the San Diego airport (6 km northwest). The wind direction (WD) (black markers) and wind speed (WS) (grey line) on February 12th was also diurnal, shifting from a light easterly land breeze (~ 1 m/s) before sunrise to a stronger westerly sea breeze (~ 3 m/s) during the day and shifting back to a light easterly land breeze after sunset. The wind data on March 13th were similar, with a difference being the absence of a shift back to easterly winds in the evening. Meteorological data from downtown San Diego (APCD) and Chula Vista (APCD) were compared on both days and agreed during the periods of sampling.

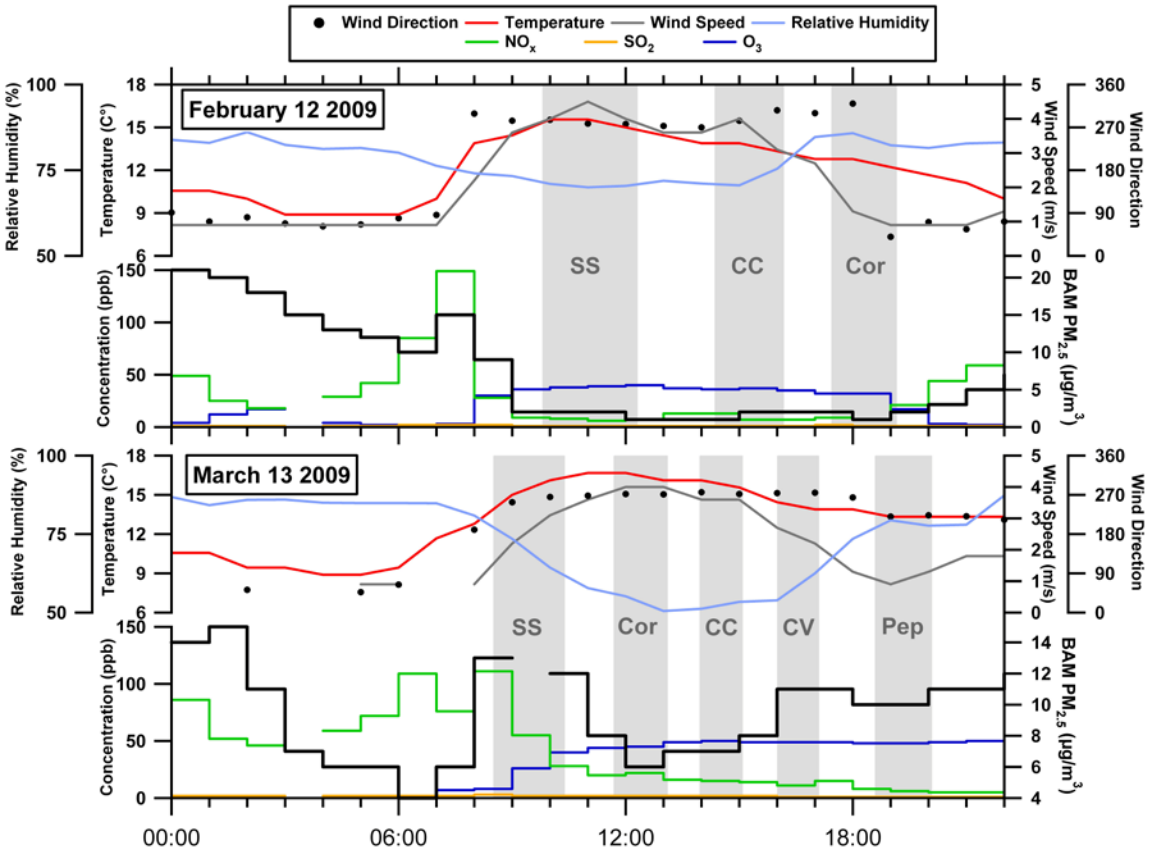

Figure 20: Comparison of meteorology conditions (temperature-red, relative humidity-light blue, wind speed-grey, wind direction-black markers) and gas phase concentrations (O_3-blue, NO_x-green, SO_2-gold) on February 12th and March 13th.

The gas phase concentrations observed on February 12th and March 13th were also similar (**Figure 20**). An increase in NO_x concentrations (green line) was observed before dawn, followed by a decrease after sunrise as O_3 concentrations (dark blue line) increased. On February 12th, the O_3 decreased after sunset and the wind shifted to a land breeze with NO_x increasing. The lack of a shift in wind direction on March 13th was accompanied by high O_3 concentrations well after dark and sustained low NO_x concentrations. On both days, SO_2 concentrations were low, and no significant patterns were observed. The similar trends in the meteorological and gas phase data suggest that differences in particle mass, number concentration, and chemistry around San Diego Bay on these two days will provide insight into sources and aging, spatially and temporally.

Air mass back trajectories were calculated using HYSPLIT 4.9 for each site during the sampling periods (130). **Figure 19a** shows the 200 meter air mass backward trajectory for the three sites sampled on February 12th (SS1, CC1, and Cor1). All three back trajectories show a strong oceanic influence with each air mass overland for less than an hour, which corresponds with the wind direction in **Figure 20a**. The air mass back trajectories calculated for March 13th are not as homogeneous, with the initial sampling site for that day (SS2) showing an air mass that was over the San Diego area for ~ 6 hours. This slow moving air mass over a region with many sources indicates that the air mass is likely polluted, while the strong sea breeze that lasted through sampling at

(Cor2, CC2, CV2, and Pep2) is indicative of cleaner conditions. The two sampling days provide an informative contrast with a relatively clean day on February 12th versus March 13th, which transitioned from polluted conditions to cleaner marine conditions. This comparison can provide information about how quickly the aerosol changes in terms of particle types present and associated secondary species (i.e. nitrate and sulfate) during clean marine wind patterns.

Particulate mass concentration is the most commonly used metric to evaluate aerosol pollution levels by state and federal regulatory agencies and has led to the development of standardized methods for determining PM_{10} and $PM_{2.5}$ mass concentrations, such as the BAM. BAM measurements at the DT-ACPD site on both days are shown in **Figure 20** (black line) and exhibit different patterns over the course of the day. On February 12th, a diurnal trend was observed with high nighttime mass concentrations (> 20 $\mu g/m^3$) that decreased in the pre-dawn hours and fell sharply after sunrise to low levels during the day (1-3 $\mu g/m^3$) with a slight increase in the late evening hours (3-5 $\mu g/m^3$). This pattern was also observed on February 10th and 11th, which were the first two non-precipitating days after five days and 43 mm of rain (February 5-9) (131). Overnight sampling at a site 21 km north of the DT site observed a similar overnight build-up in $PM_{2.5}$ with size distribution data (SMPS and APS). This increase in $PM_{2.5}$ is likely local as back trajectory analysis shows an oceanic origin, indicating that elevated $PM_{2.5}$ levels were likely not transported. On March 13th a peak in mass concentration between 08:00-10:00 PST related to morning rush hour was observed, but there was not a clear diurnal trend as $PM_{2.5}$ concentrations did not drop sharply to minimal levels during the day. $PM_{2.5}$ concentrations were >5 $\mu g/m^3$ throughout the day with levels of ~10 $\mu g/m^3$ from late afternoon through the evening (16:00-23:00 PST). The distinctly different temporal trends (high to very low on February 12th and higher, but less diurnal on March 13th) of $PM_{2.5}$ mass concentration on days with similar meteorological and gas-phase temporal patterns indicate differences in particle properties and dynamics, epitomizing the difficulty in understanding the urban aerosol.

b. Variability of Particle Mass and Number Concentrations

To determine whether the mass concentrations observed at the downtown site were representative of particle mass at different points around the San Diego Bay, the ATOFMS $PM_{2.5}$ mass concentration (blue bars), and BAM $PM_{2.5}$ mass concentrations at the mobile ATOFMS laboratory sites (red bars) were compared with BAM measurements at the downtown site (green bars) (**Figure 21a**). On February 12th, the $PM_{2.5}$ concentrations for the downtown BAM and the trailer BAM match at 1 $\mu g/m^3$ (SS1, CC1, and Cor1). The ATOFMS mass concentrations are quite different from the trailer BAM and DT-APCD BAM concentrations at SS1, which we believe to be related to counting issues with the APS related to freshly generated sea salt particles from the ocean, which was 50 meters west of the sampling site. However, the measurements agree at the CC1 and Cor1 sites, where there was less of an influence from sea spray. During this period number concentrations (**Figure 21b** – orange bars) were also low (1865-4169 $\#/cm^3$). We believe this agreement is due to clean conditions resulting from the 5 days and 43 mm of rain in the week before sampling (February 5-9) mentioned above, which decreased concentrations of larger particles (i.e. > 0.5 μm) and led to similar conditions among larger particles around the bay.

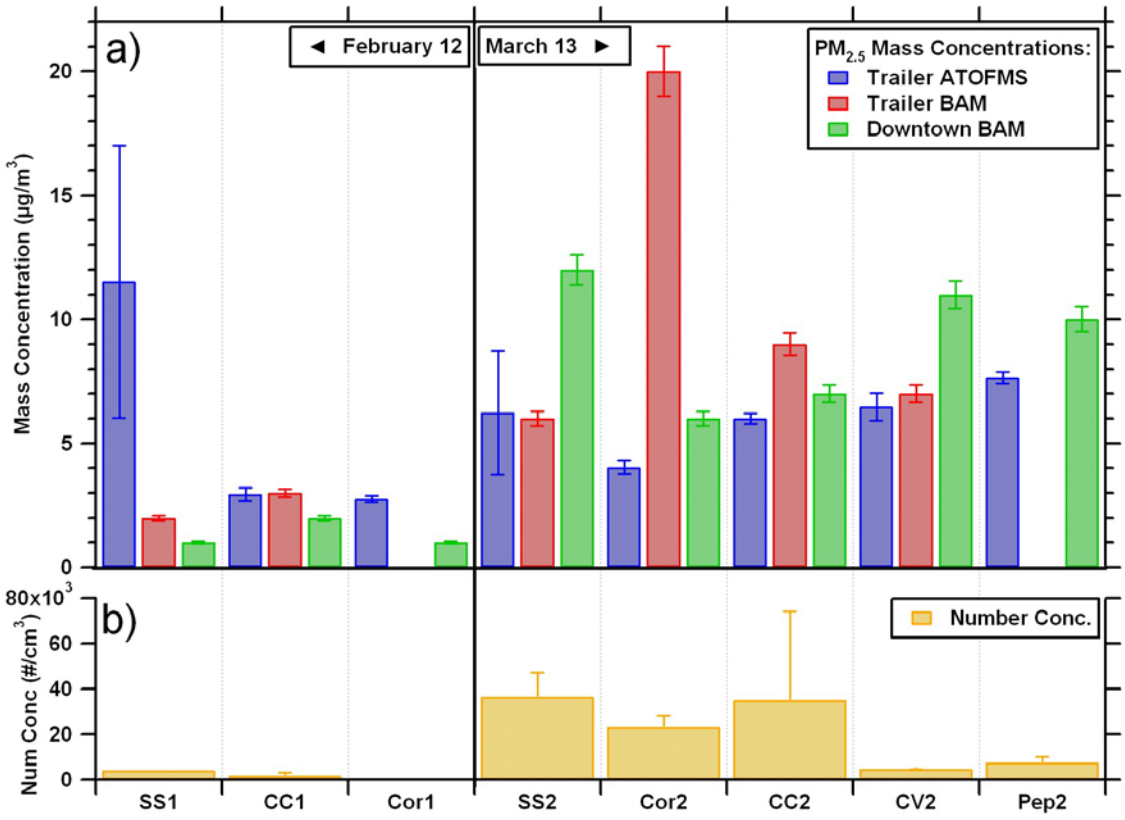

Figure 21: (a) $PM_{2.5}$ mass concentration data at each site for the: Scaled ATOFMS mass (blue bars), trailer BAM (red bars), and DT-APCD BAM (green bars). (b) Number concentration by site from summed SMPS scans (gold bars).

On March 13th the relationships between the mass measurements are more complex. At SS2, the trailer mass concentrations (ATOFMS and BAM) match within error, while the concentrations downtown are much higher. The Cor2 site had an anomalous BAM reading, but the Cor2 APS and DT mass measurements are similar for these sites that are ~1.5 km apart. The CC1 site has similar agreement between all three $PM_{2.5}$ measurements (distance between CC and DT ~0.6 km). The trailer measurements agree well at the CV2 site, but are quite different than the downtown site (distance ~ 4 km). Lastly, the ATOFMS mass is somewhat lower at the Pep2 site than the DT site (distance ~ 4 km), but more similar than at the CV2 site (the trailer BAM had a flow error at Pep2). Overall, at sites closer to downtown, there is better agreement between the trailer $PM_{2.5}$ and DT-ACPD $PM_{2.5}$, but the trailer $PM_{2.5}$ is smaller than DT mass when the distance between mobile and DT-APCD site were greater in the morning and late afternoon. Despite variations around the bay, these mass measurements indicate a background level of particulate matter mass, which is likely related to there being essentially no rain (only 1 day and <0.04 inches) between February 12th and March 13th. The similarity in mass concentrations throughout the day on March 13th does not match with the variability in particle number concentration and chemical composition observed with the SMPS, APS, and ATOFMS.

The number concentrations on March 13th have spatial and temporal variability. Temporally the SS2 or CV2 sites would be expected to have the highest number

concentrations as they were sampled during morning and evening rush hour, as well as SS2 having a back trajectory that spent significantly more time over the city than the other four. This initial hypothesis is correct with SS2, but far off with CV2. Spatially, the CC2 site is located closest to the source region of downtown San Diego and the San Diego Port. The number concentration observed at this site is higher than would be expected temporally, as concentrations should decrease during the day as winds shift to coming from the ocean, thus the increased concentration at CC2 shows spatial variation around the bay. CC2 also has the highest standard deviation of number concentrations indicating that the downtown aerosol is dynamic even over 1 hour of sampling. Thus, a gradient from north to south along the bay with higher concentrations downtown and lower concentrations to the south is hypothesized to exist during strong sea breezes and oceanic air mass back trajectories, while land based air masses such as SS2 are not necessarily expected to follow this trend. This is consistent with the many particle sources densely packed in the downtown area, while sources are less concentrated geographically as you travel out from downtown to the other sampling sites.

c. Variation in Aerosol Size Distributions

Size distributions were analyzed for both February 12th and March 13th (**Figure 22**). **Figure 22a** shows SMPS and APS size distributions measured on February 12th (SMPS measurements are not available for Coronado on this date), while **Figure 22b** shows similar measurements from March 13th. The aerosol number concentrations shown in **Figure 22a** are lower than those in **Figure 22b**. The concentrations are somewhat intuitive: SS1 is a coastal site that had a strong sea breeze during sampling leading to a higher concentration of larger particles (i.e. sea salt), while CC1 is an urban site in close proximity to major freeways and other sources leading to more small particles (0.010-0.030 μm) and fewer large particles (>0.030 μm). The APS traces for CC1 and Cor1 are also nearly identical as would be expected for two sites ~1.5 km apart on a day with somewhat homogeneous conditions for larger particles (> 0.5 μm) due to wash out of large particles by rain the previous days.

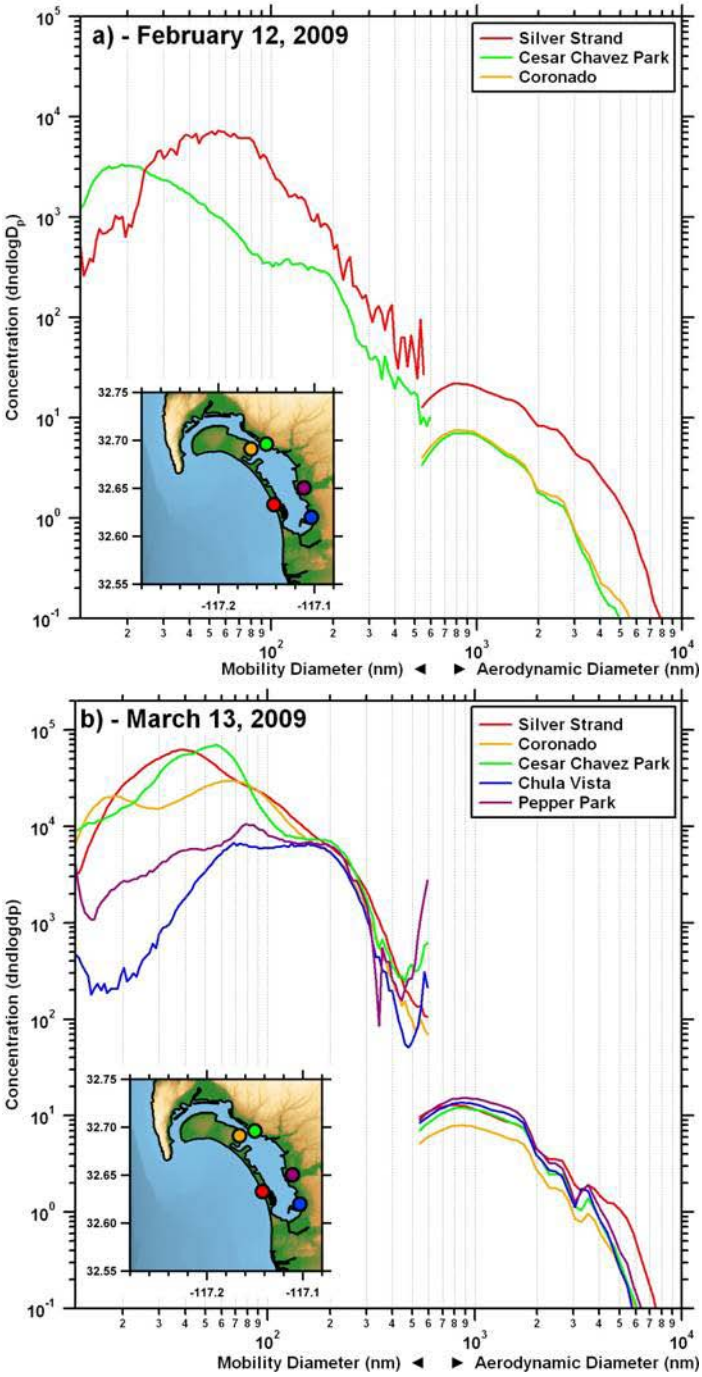

Figure 22: Size distribution measurements (SMPS and APS) for February 12th and March 13th as measured at the trailer sampling sites. The red traces correspond to Silver Strand, green traces to Cesar Chavez Park, yellow to Coronado, blue to Chula Vista, and purple to Pepper Park

A distinctive feature of **Figure 22b** is that the SMPS size distributions observed on March 13th show a great deal of variability. The small mode and relatively high number concentrations observed at Cor2 (18.8 nm and 23,103 #/cm^3) are likely the result of close proximity to a major highway (< 50 m south) and the larger modes and lower number concentrations at CV2 (68 nm and 4,745 #/cm^3) and Pep2 (79 nm and 7,609 #/cm^3) are the result of more distant sources and an older aerosol. The high number

concentration at SS2 (36,613 #/cm^3) is related to the air mass back trajectory as described above. Lastly, the high number concentration (34,928 #/cm^3) and standard deviation of number concentration (39,005 #/cm^3) (shown as error on **Figure 21b**) at CC2 indicate the dynamic nature of the sources.

An important aspect of **Figure 22** is that the size distributions on February 12th in the overlap region between the SMPS and APS (0.523-0.604 μm) are within instrumental error at those sizes, but there is a large disconnect in the overlap region between the SMPS and APS measurements on March 13th that is beyond error. This is due to the fact that the SMPS measures electrical mobility diameter (d_m) and the APS measures aerodynamic diameter (d_a). These two parameter are related to one another by the following equation (132) where ρ_0 is the unit density (1 g/cm^3), ρ_p is the particle density, and χ is the shape factor:

$$\frac{d_a}{d_m} = \sqrt{\frac{\rho_p}{\chi \rho_0}} \tag{0.1}$$

As can be seen from the equation, as shape factor approaches 1 (spherical) and density approaches the unit density, aerodynamic and electrical mobility diameter converge. This indicates that particles in the overlap region on February 12th were both spherical and had taken up large amounts of water, as shown previously by Spencer et al. when atmospheric liquid water content increased, effective density approached unity (48). By comparison, on March 13th there is a multiple order of magnitude difference in number concentration in the overlap region indicating an aerosol that likely has non-unity density and shape factor, as mobility and aerodynamic diameter give different distributions. These differences show that particles are either denser, less spherical, or both when compared to the February 12th aerosol, indicating that the aerosol on March 13th is neither well-mixed nor homogeneous. This is a key point as high aerosol concentrations in urban environments are frequently assumed to be homogeneous due to atmospheric processing, but these results indicate that this is not a safe assumption.

d. Differing Aerosol Sources Determined by Particle Chemistry

The main particle types observed at the different sampling sites included: sea salt, dust, elemental carbon mixed with organic carbon, organic carbon, and biomass particles. These particle types have been described for the San Diego area previously (74,133). Briefly, sea salt particles were identified by $^{23}Na^+$, $^{62}Na_2O^+$, $^{63}Na_2OH^+$, and $^{81,83}Na_2Cl^+$; dust particles were identified by peaks corresponding to $^{23}Na^+$, $^{27}Al^+$, $^{39}K^+$, $^{56}Fe^+$, $^{-76}SiO_3^-$, and $^{-77}HSiO_3^-$; elemental carbon particles mixed organic carbon (ECOC) were characterized by peaks at ($^{12}C_1^+$, $^{24}C_2^+$,…, C_n^+) with less intense organic carbon markers ($^{27}C_2H_3^+$, $^{29}C_2H_5^+$, $^{37}C_3H^+$, and $^{43}C_2H_3O^+$); organic carbon (OC) particles had high intensity peaks at $^{27}C_2H_3^+$, $^{29}C_2H_5^+$, $^{37}C_3H^+$, and $^{43}C_2H_3O^+$, as well as many other carbon fragments; and biomass particles identified by a strong potassium peak ($^{39}K^+$) and minor organic carbon ion markers. Mixing state of different particle types with markers for clean (chloride) and aged (nitrate and sulfate) particles will be discussed below.

The relative mass fractions for submicron and supermicron particle types are shown **Figure 23a** and **Figure 23b** respectively, with the black markers representing the total ATOFMS mass concentration at each site for that size range. In **Figure 23a** the very low concentrations of non-sea salt particle types (less than 10% at each site) on February

12th (SS1, CC1, Cor1) indicate very clean conditions, as discussed above. On March 13th between 25-50% of the particle mass under 1 μm are not sea salt particles, but rather carbonaceous particles (OC, ECOC, and biomass) indicating significant anthropogenic particle concentrations. This is significant as each site was within 200 meters of the salt water bay and heavily impacted by sea salt particles. On March 13th there is a decrease in mass for the OC particle type during the day, while ECOC and biomass are present throughout the day. The higher mass fraction of the OC particle type at SS2 was related to the different air mass history discussed above. As the sea breeze strengthens during the day, the OC particle type decreases to negligible levels by the time sampling is conducted at CV2 and Pep2, indicating the importance of temporal variation. The combined fraction of mass from ECOC and biomass particles is substantial throughout the day (14-32%), indicating particle types that are part of the urban background. The supermicron mass concentrations and mass fractions (**Figure 23b**) are remarkably consistent during the 8 time periods over 2 different days. This indicates that a large fraction of the spatial and temporal variability in particle number concentration and chemical composition is caused by the submicron particles.

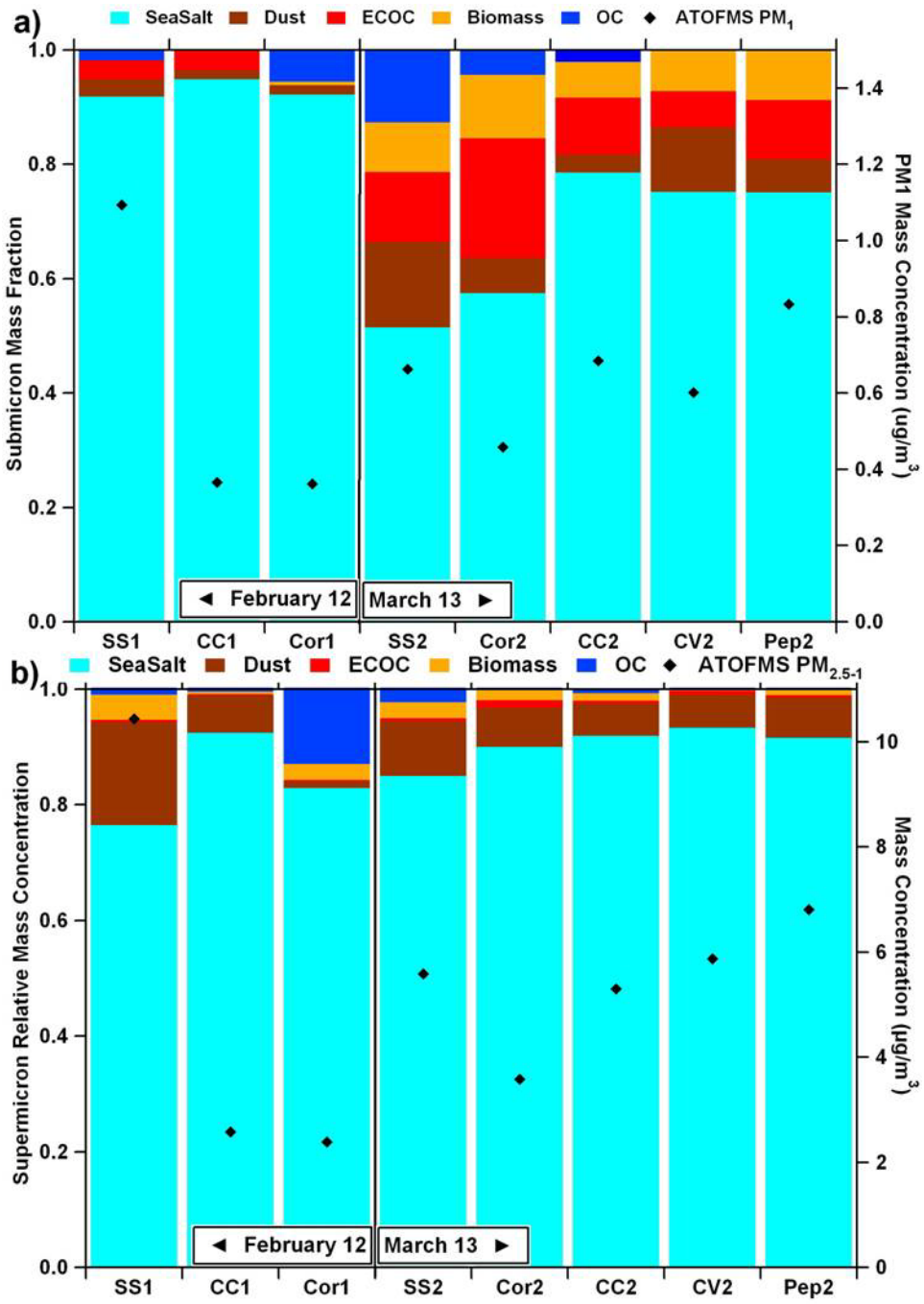

Figure 23: Chemically-resolved relative mass fractions of particle types for (a) submicron (0.523 – 1 µm) and (b) supermicron (1-2.5 µm) particles at each site. The black diamonds represent the ATOFMS mass concentration by site.

e. Differences in Particle Aging and Mixing State

With respect to aging, mass spectral markers for chloride ($^{-35}Cl^-$), nitrate ($^{62}NO_3^-$), and sulfate ($^{97}HSO_4^-$) can provide information as to the degree and form of particle aging, as nitrate and sulfate can be markers of secondary processing. Chloride has been shown as a good marker for unreacted sea salt particles, while nitrate has been shown as a

marker for aging on many particle types (134,135). Sulfate is identified by the $^{97}HSO_4^-$ peak (136), except for sea salt particles where there is interference from the $^{23}Na^{37}Cl_2^-$ at m/z -97. Amongst different particle types, the aging and secondary species change temporally and spatially. **Figure 24a** shows the average nitrate and chloride peak areas at each site for sea salt particles, while **Figure 24b** and **Figure 24c** show nitrate and sulfate for biomass and ECOC particles, respectively. The February 12th sampling show higher chloride peak area for sea salt at all 3 sites, while on March 13th the nitrate peak area starts larger and decreases to roughly even with chloride during the day, suggesting fresh unreacted particles (**Figure 24a**). While there were not enough biomass and ECOC particles with negative mass spectra to analyze peak areas on February 12th, on March 13th nitrate is seen to decrease during the day similar to sea salt, indicating that the particles are either less aged or have had nitrate volatilize (**Figure 24b** and **Figure 24c**). For biomass, sulfate peak area becomes larger throughout the day on March 13th. This may be related in part to the strong ocean breeze observed for Cor2, CC2, CV2, and Pep2, which has had less time to react heterogeneously and take up nitrate. **Figure 24d** shows the ratio of the sulfate peak area and nitrate peak area at each site during the day. The ratio increases throughout the day for both particle types. The lower nitrate concentrations suggest that nitrate may not have been present on the particles sampled at CC2, CV2, or Pep2 due to cleaner conditions later in the day. Another possibility is that due to its semi-volatile nature, nitrate may have partitioned back to the gas phase in the late afternoon due to higher temperatures (137).

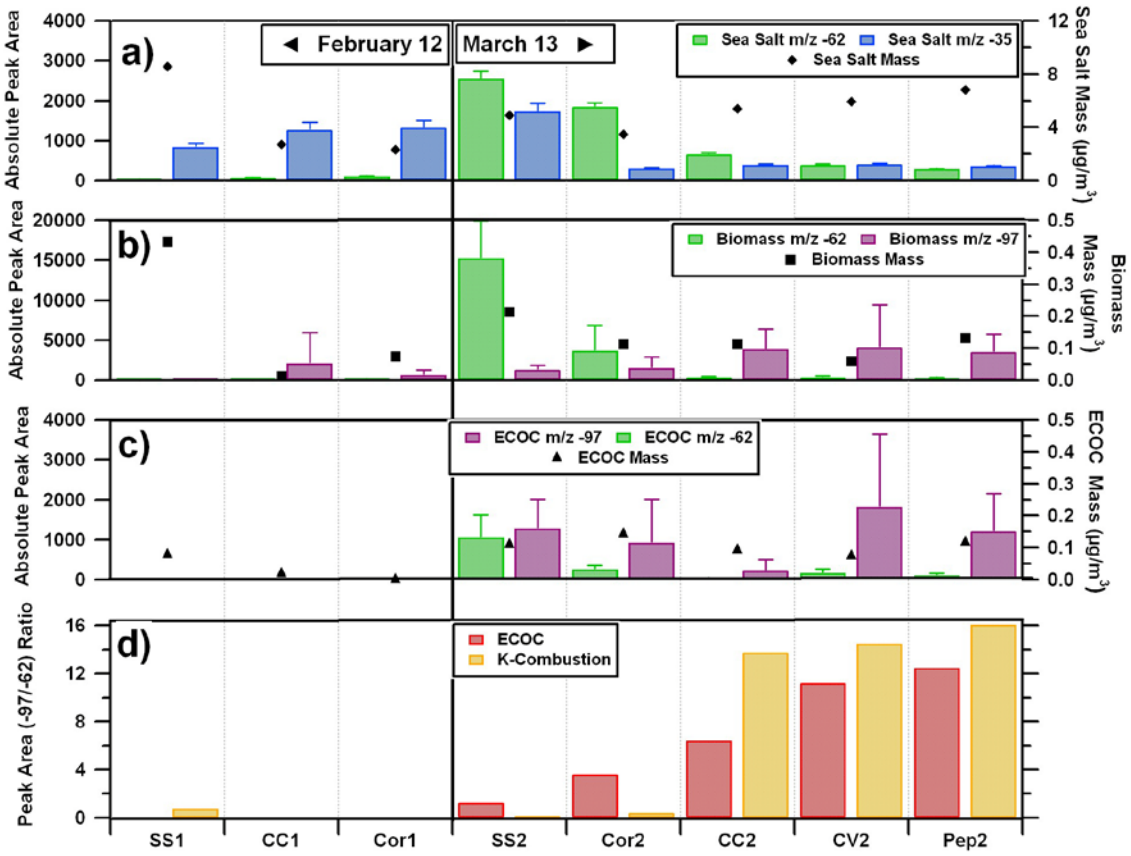

Figure 24: Peak areas related to aging for (a) Sea salt particles, (b) Biomass particles, and (c) ECOC particles. For sea salt particles, chloride (blue – $^{35}Cl^-$) and nitrate (green –$^{62}NO_3^-$) are plotted. For biomass and ECOC particles, nitrate and sulfate (purple – m/z $^{97}HSO_4^-$) are plotted. The ratio of the peak areas for nitrate and sulfate (d) are given for biomass and ECOC particle types.

f. Variations in Chemistry and Implications for Models and Regulations

The measurements described above show that even on days with relatively similar meteorological conditions there can be considerable differences in particle mass and number concentrations and chemical mixing state within a marine-influenced urban atmosphere. During clean conditions similar mass concentrations, number concentrations, and particle chemistry were observed. During polluted time periods a strong diurnal pattern was observed with respect to particle types (decreasing organic carbon) and secondary species (nitrate) associated with the background particle types changed. Spatially, the downtown area represented a source region after the wind shift, as indicated by the size distributions and number concentrations, which fed into a general background level of particulate matter that appears to have built up over a month long period without rain. However, temporal patterns are shown to have a greater impact on particle properties than spatial patterns on this city-wide scale.

Submicron particles are more likely than supermicron particles to be inhaled and deposited into the tracheobronchial and pulmonary regions of the body than the naso-oro-pharyngo-laryngeal regions (138), which suggests that understanding the sources and

processing contributing to the urban aerosol is critical to determining the degree to which it impacts human health. The initial deployment of the mobile ATOFMS laboratory and single particle measurements from this platform demonstrate the importance of understanding these fluctuations in particle chemistry as they relate to sources and aging processes. The difference between a very clean day (February 12th) and a day with higher mass concentrations (March 13th) is shown by a less homogeneous aerosol that varies diurnal, more than spatially. The relative importance of temporal over spatial variation is only expected to increase as mass concentrations increase, except in close proximity to strong particle sources. Describing the urban aerosol from a single particle mixing state perspective will be a key to improving future models that will analyze the links between aerosol concentration and composition and their impact on human health. When crafting future regulations the vast variation possible within similar $PM_{2.5}$ mass concentrations needs to be considered and methods with higher time resolution chemical information are necessary as attempts are made at bridging the causal gap between air pollution and health.

iv. Acknowledgements

Andrew Ault acknowledges the Unified Port of San Diego Environmental Services Department for funding sampling with a graduate research grant. Joseph Mayer is thanked for his efforts with adapting the trailer and installing the generators. Additional funding was provided by the California Air Resources Board under contract 04-336. The authors gratefully acknowledge the NOAA Air Resources Laboratory for the provision of the HYSPLIT transport model and READY website used in this publication.